ISBN: 978-628-96613-3-0. ISSN: 2414-6390. Digital Object Identifier: https://dx.doi.org/10.18687/LACCEI2026.1.1.892

Numerical Modeling of Cantilever and Geogrid-Reinforced Retaining Walls with Planar Geodrain in Granular Soils of Sachaca–Arequipa Using PLAXIS 2D

Jeremy D. Amado[1], Heilyn V. Choque[1], H. Saul Perez-Montaño1
Universidad Tecnológica del Perú, Facultad de Ingeniería Civil, Arequipa-Perú,
U19303015@utp.edu.pe, 1620596@utp.edu.pe, C30774@utp.edu.pe

Abstract– Mass movements represent a critical geotechnical challenge in seismic zones such as Sachaca, Arequipa, where the vulnerability of sandy–clayey soils demands efficient retaining solutions. This study compares the performance of reinforced-concrete cantilever retaining walls and mechanically stabilized earth (MSE) walls reinforced with biaxial geogrid and planar geodrain, using numerical modeling in PLAXIS 2D. Soil properties were characterized (moisture content 31.62%, friction angle 30.1°), and stresses, deformations, and pore pressure were evaluated. The results show that cantilever walls exhibit lower displacements and deformations, while MSE walls provide superior pore-pressure relief (≈1.12 times). These findings offer technical criteria to optimize the design of retaining structures in granular soils of seismic regions in southern Peru.

Key words: Retaining *wall, PLAXIS 2D, biaxial geogrid,* planar geodrain

I. INTRODUCTION

Mass movement is one of the main geotechnical challenges due to its effects on infrastructure, the economy, and public safety. This phenomenon is associated with seismic activity, geological conditions, and vibrations, which demand robust and adaptable engineering solutions [1]. In the district of Sachaca (Arequipa, Peru), geological studies report highly vulnerable soils, generating significant risks for buildings and the local population [2]. The recent slope instability at the Tío Grande sports complex highlights the need to implement retaining systems compatible with local geotechnical and seismic conditions [3].

Cantilever reinforced-concrete retaining walls have traditionally been used, with designs based on safety factors against overturning, sliding, and bearing capacity [4][5]. In recent decades, mechanically stabilized earth (MSE) walls have gained relevance due to the use of geosynthetics such as geotextiles, geogrids, and geodrains [5][8]. These solutions offer advantages in construction speed, adaptability, and cost, with reductions of up to 15% and improvements in stability [9]–[11]. In low-permeability soils, consolidation and pore pressure influence long-term performance, making drainage efficiency through geodrains a critical factor [12], [13].

The design and analysis of retaining walls has been addressed through numerical tools such as PLAXIS 2D and 3D [14]–[16]. However, no studies are available that comprehensively compare the behavior of cantilever walls and MSE walls reinforced with geogrid and geodrain under the specific geotechnical and seismic conditions of Sachaca. Soil spatial variability, surcharge loads, and drainage efficiency are critical factors in vulnerable urban areas [17]–[24]. This study evaluates the performance of cantilever walls and reinforced MSE walls through numerical modeling in PLAXIS 2D, considering lateral displacements, stresses, and drainage efficiency. The objective is to identify the most suitable alternative for granular soils in seismic zones such as Sachaca, optimizing safety and material use.

II. METHODOLOGY

2.1 Soil Characterization

The geotechnical characterization of the soil was carried out based on the technical report corresponding to the Sachaca area [26], applying ASTM-standardized tests to determine its physical and mechanical properties. The grain-size analysis, performed according to ASTM D422-63, established the particle-size distribution using sieves down to No. 200 [27]. The moisture content was determined following ASTM D2216-19 by oven-drying the sample at 110 ± 5 °C and calculating the mass loss as the water percentage [28]. The SUCS classification, according to ASTM D2487, identified the material as silty sand (SM), while the Atterberg limits were obtained following ASTM D4318, using the Casagrande device for the liquid limit and the rolling method for the plastic limit [29], [30]. The direct shear test, conducted in accordance with ASTM D3080-11, allowed the evaluation of the drained and consolidated shear strength of the samples [31]. The results indicated a sandy-clayey soil with a moisture content of 31.62% and an internal friction angle of 30.1°, parameters essential for numerical modeling in Bentley PLAXIS 2D Ultimate 2024.1.0.

2.2 Design of retaining walls

The cantilever reinforced concrete wall (RCW) and the mechanically stabilized earth (MSE) wall reinforced with geogrid and geodrain were designed, taking into account the acting loads and a uniform surcharge of 0.5 ton/m. The bearing capacity of the soil was determined based on its geotechnical characteristics, assuming a continuous footing typical of retaining walls and applying Equation (1) for its evaluation.

$$q_u = cN_c + qN_q + \frac{1}{2}\gamma BN_\gamma \qquad (1)$$

Obtaining a bearing capacity ofq_u= 3.23 Kg/cm^2.

2.3 Cantilever reinforced concrete retaining wall (MV)

2.3.1 Preliminary sizing

The preliminary sizing stage establishes the general dimensions of the wall prior to detailed design. This step is essential to ensure the structural stability of the cantilever reinforced concrete retaining wall (MV), using the equations provided in Table I.

TABLE I
PRELIMINARY SIZING

Wall height	$H = D_f + h$ (2)
Wall Top	$0.20 \leq t_1 \leq 0.30$ (3)
Width	$B = 0.60\ x\ H$ (4)
Stem thickness	$h_z = H/10$ (5)
Toe	$P_{min} = \frac{B}{4}\ P_{max} = \frac{B}{3}$ (6)
Heel	$T = B - (P + t_2)$ (7)

Note: The total wall height H is defined as the sum of the excavation depth D_f and the height of the retained soil up to the stem h, according to Equation (2). The thickness of the top section t_1 is adopted based on the values established in Equation (3). The base width is determined from the height H by substituting its value into Equation (4). The stem footing thickness h_2 is calculated using Equation (5). The toe length P is obtained using the width defined in Equation (3), which is then substituted into Equation (6). Finally, the heel length T is determined from the values obtained in Equations (3), (4), and (6), substituting them into Equation (7) [32].

2.3.2 Concrete and Steel Properties.

For the construction of the cantilever retaining wall, specific requirements were established for the concrete and reinforcing steel to ensure structural stability and load-carrying capacity. The concrete was specified with a compressive strength fc′ of 210 kg/cm², and its unit weight was also considered in the evaluation of the acting loads. The reinforcing steel was defined with a yield strength Fy of 4,200 kg/cm², a key parameter for resisting the tensile and bending stresses induced in the structure. The proper selection and specification of these materials is essential for the safe design and construction of the retaining wall.

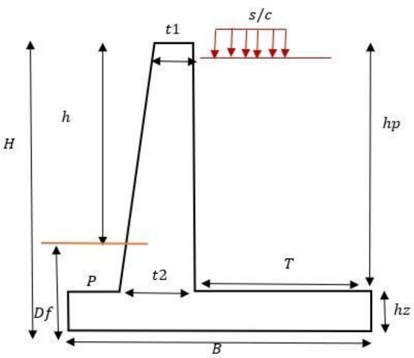

Fig. 1. Profile view of the components of the MV listed in Table I.

2.3.3 Active Rankine Earth Pressure.

The Rankine active earth pressure corresponds to the lateral pressure exerted by the soil on a retaining wall when the wall undergoes sufficient displacement for the soil mass to reach a plastic equilibrium state, known as the Rankine failure condition. In this state, the soil expands laterally, reducing the pressure acting on the wall and generating an inclined failure plane whose orientation depends on the material's internal friction angle. This model is a fundamental criterion in the design of retaining walls, since the Rankine active pressure represents the minimum lateral load that the structure must resist to ensure stability. The active earth pressure from the backfill is considered to act at one-third of the wall height, measured from the base [32].

2.3.4 Stem design.

The design of the stem of a cantilever retaining wall consists of sizing and reinforcing the vertical portion of the structure, also known as the stem or shaft. This element behaves as a cantilever slab, resisting the lateral earth pressure. The design focuses on determining the thickness and the amount of reinforcing steel required to withstand the bending and shear forces generated by the soil pressure. This process involves calculating the loads, performing a structural analysis of the wall to determine the maximum moments and shear forces, and finally specifying the steel reinforcement to ensure the safety and performance of the structure. To achieve this, the formulas in Table II are applied.

TABLE II
DESIGN EQUATIONS FOR THE STEM OF A RETAINING WALL

Active coefficient	$Ka = tan^2\left(45º - \frac{\emptyset}{2}\right)$	(8)
Equivalent height S/C	$h_s = \frac{s/c}{Ys}$	(9)
Moment	$M_u = 1.7\left[\frac{Ka*Ys*hp^2}{2} * \left(\frac{hp}{3} + 3\right)\right]$	(10)
Effective depth	$d = \sqrt{\frac{M_u}{\emptyset*b*f'c*w*(1-0.59*w)}}$	(11)
Throat (t_2)	$t_2 = d + r + \frac{\emptyset}{2} * As$	(12)

Note: To obtain the active coefficient (Ka), the internal friction angle (φ) is used and substituted into Equation (8). The equivalent height (hs) is determined from the surcharge (s/c) divided by the soil unit weight (γs) and substituted into Equation (9). The moment (Mu) is calculated using the values from Equations (8) and (9), substituting them into Equation (10). The effective depth (d) is determined from the result of Equation (10), the flexural coefficient 0.90, the balanced reinforcement ratio, and the concrete strength f'c of 210 kg/cm²; all of these are entered into Equation (11). The throat thickness (t2) is obtained from the result of Equation (11), which is substituted into Equation (12), considering a concrete cover of 4 cm [32].

2.3.5 Shear verification at the base of the wall

The shear verification at the base of retaining walls is a fundamental step in structural design, intended to ensure that the basal section of the wall has the required capacity to withstand the horizontal forces induced by earth pressure, thereby preventing shear failure, or sliding. This analysis is performed by comparing the acting shear force Vu, generated by the lateral soil pressures, with the nominal shear strength of the section Vn, which results from the combined contribution of the concrete and the reinforcing steel. The design is considered adequate when the acting force is less than or equal to the nominal strength reduced by the corresponding safety factor, thus ensuring the structural stability of the wall. The verification of shear forces at the base of the wall is carried out using the expressions provided in Table III.

TABLE III
SHEAR-VERIFICATION FORMULAS

Ultimate shear calculation	$V_u = 1.7\left(Ka * \gamma s * (hp - d)\left(\frac{1}{2}(hp - d) + hs\right)\right)$ (13)
Concrete shear calculation	$V_c = 0.53 * \sqrt{fc} * b * d$ (14)
Verification	$Vu \leq Vc$ (15)

Note: For the ultimate shear calculation, the results from Equations (9) and (11) are used in Equation (13). For the concrete shear calculation, the value obtained from Equation (11) is substituted into Equation (14) [32].

2.3.6 Verifications

The factor of safety (FS) in retaining walls is a fundamental indicator of structural stability, defined as the ratio between the resisting forces and the acting forces that tend to cause system failure. Its evaluation is essential to ensure an adequate safety margin against the main failure modes, which include overturning, sliding, and bearing-capacity failure of the soil. Verifying that the obtained safety factors exceed the minimum required values confirms that the wall can safely and reliably withstand the acting loads throughout its service life. Likewise, this analysis validates the adequacy of the adopted preliminary design, using the expressions provided in Table IV.

TABLE IV
SAFETY-FACTOR FORMULAS

Friction force	$fr = \sum F_v * \tan(\phi_s)$ (16)
Sliding F.S.	$F.S.D = \frac{fr}{\sum F_h} \geq 1.5$ (17)
Overturning F.S.	$FS_v = \frac{\sum MF_v}{\sum MF_h} \geq 1.5$ (18)

Note: To determine the friction force (fr), the internal friction angle (φ) and the overturning force (Fv) are substituted into Equation (16). For the sliding F.S., the value obtained from Equation (16) is used together with ∑Fh (horizontal earth pressure) in Equation (17). For the overturning F.S., the ∑MFv (vertical moments) and ∑MFh (horizontal moments) from the table are considered and substituted into Equation (18) [32].

2.4 MSE with geogrid and geodrain.

A mechanically stabilized earth (MSE) wall is a retaining structure composed of successive layers of granular backfill reinforced with geogrids. These geogrids, made of high-tensile-strength geosynthetic materials, interact with the soil through friction and confinement mechanisms, increasing the system's bearing capacity and improving its resistance to lateral earth pressure. Complementarily, the incorporation of a geodrain behind the wall enables the collection and discharge of infiltrating water, reducing hydrostatic pressure and contributing to the structural performance and long-term durability of the system.

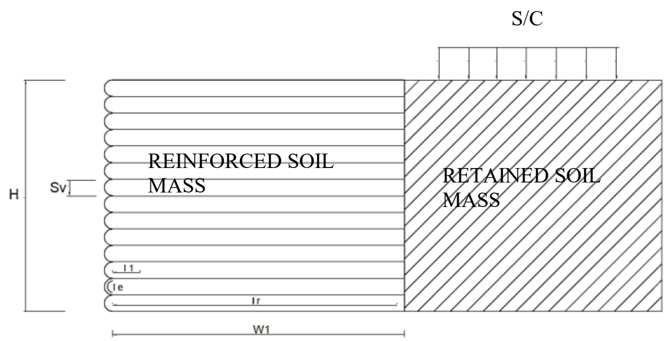

Fig. 2. Profile view of the components of the MSE listed in Tables V and IV.

2.4.1 Soil properties

A soil study is a technical investigation carried out to determine the properties of the soil and the subsurface conditions at a construction site. Boreholes and laboratory tests are used to identify characteristics such as grain size distribution, friction angle, and soil bearing capacity. This process is essential to ensure a safe and appropriate structural design for the site conditions, as documented in a geotechnical report [26].

2.4.2 Internal Stability

Internal stability of a retaining wall refers to the ability of its own components to withstand the forces acting within the structure, preventing failures due to tension, shear, deformation, or rupture of its constituent elements. This criterion focuses on the strength of the reinforcement—such as geogrids in mechanically stabilized earth walls or steel in reinforced concrete walls—and on the integrity of their connections. In general terms, internal stability ensures that the materials and joints possess sufficient capacity to resist the internal demands generated by earth pressure and the applied external loads [32]. This can be verified using the equations presented in Table V.

TABLE V
EQUATIONS OF INTERNAL STABILITY

Rankine σ' coefficient	$K_a = tan^2\left(45º - \frac{\phi}{2}\right)$	(19)
Active pressure	$\sigma'_a = K_a \gamma_1 z$	(20)
Allowable geogrid tension	$T_{per} = \frac{T_{ultm}}{RF_{id} * RF_{cr} * RF_{cdb}}$	(21)
Vertical spacing	$S_v = \frac{T_{pet}}{\sigma'_a * FS_b}$	(22)
Rankine failure-zone length	$l_r = \frac{H - s_v}{tan(45º - \frac{\phi}{2})}$	(23)
Effective length	$l_e = \frac{S_v K_a FS_p}{2\tan(f_i)}$	(24)
Length of each layer	$L = l_r + l_e$	(25)
Overlap length	$l_1 = \frac{S_v K_a FS_p}{4\tan(f_i)}$	(26)

Note: The value of the friction angle (φ) obtained from Equation (19) is substituted into Equation (20). The ultimate tensile strength (Tult) is substituted into Equation (21). In Equation (22), the vertical spacing (Sv) is determined using the results from Equations (21) and (20). In Equation (23), the Rankine failure-zone length (lr) is calculated using the data from Equation (22) and the friction angle (φ), which allows the failure condition of the soil to be defined under the previously described conditions. Furthermore, the effective length (Le), or the longitudinal development of the geogrid, is obtained from Equation (24) using the results from Equations (22) and (19), and the friction angle multiplied by 2/3, which corresponds to fi. To determine the layer length (L), or per level, in Equation (25), the values from Equations (23) and (24) are substituted. Finally, the overlap length (L1), which corresponds to the coverage between layers, is calculated using the data from Equations (22), (19), and fi [32].

2.4.3 External stability

External stability in a retaining wall refers to the ability of the structure, considered as a rigid block, to resist overturning, sliding, and bearing-capacity failure of the foundation soil. The analysis focuses on ensuring that the wall as a whole does not fail when interacting with external soil forces, according to the equations presented in Table VI.

TABLE VI
EXTERNAL STABILITY EQUATIONS

Active force	$P_a = \frac{1}{2} H^2 K_a \gamma$	(27)
Overturning verification	$FS_{vuelco} = \frac{M_R}{M_O} = \frac{W_1 x_1}{P_a * \frac{H}{3}}$	(28)
Sliding check	$FS_d = \frac{(W_1) * \tan(k\phi)]}{P_a}$	(29)
Ultimate load	$q_u = c_\gamma N_c + \frac{1}{2}\gamma_2 L N_g$	(30)
Vertical stress	$\sigma'_{o(H)} = \gamma_1 H$	(31)
Ultimate bearing-capacity failure	$FS_{cu} = \frac{q_{ult}}{\sigma'_{o(H)}}$	(32)

Note: The value of Ka obtained from Equation (19) is substituted into Equation (27) to determine the active force (Pa). Then, for the overturning verification (overturning F.S.), the result from Equation (28) is used and compared with the required safety factor, which must be equal to or greater than 3. Next, using the friction angle and the value from Equation (27), Equation (29) is evaluated for the sliding check (sliding F.S.), which must be equal to or greater than 1.5. Finally, Equation (30) is used to calculate the ultimate load (qu) based on the friction angle. With the results from Equations (30) and (31), the vertical stress is obtained in Equation (32), and the value is checked to ensure it falls within the minimum range of 3 to 5 [32].

2.4.4 Geodrain selection

Para seleccionar el geodrén, el mismo debe soportar el peso que se ubique encima del mismo [32], [33]

$$FS_c = \frac{compressive\ strength}{W_1} \qquad (33)$$

Where the minimum FSc is 1.25

2.5 Parametric study

The dimensions and conditions of cantilever walls (CW) and mechanically stabilized earth (MSE) walls reinforced with geogrid and geodrain directly influence their structural and geotechnical behavior. In this study, the total height of the walls, the groundwater limit and level, the properties of the backfill and geosynthetics, as well as the general geometry and the applied surcharge, were kept constant. Two key parameters were varied: the vertical spacing of the geogrid in the MSE walls and the stem thickness at the top (corona) in the cantilever walls. These variations produced six different analysis configurations.

III. RESULTS

3.1 Geotechnical characterization of the soil

The grain-size distribution curve in Figure 2 reveals a predominantly sandy material with a continuous gradation and minimal gravel content. The curve begins with nearly 100% passing at the 19.1 mm sieve, confirming the absence of coarse particles. A gradual decline in passing percentage is observed across the sand fraction, with approximately 64% passing at the 0.30 mm sieve (No. 50). The curve steepens near the finer range, where 21.6% of the sample is retained on the No. 200 sieve (0.074 mm), leaving 17.7% passing—indicating a significant silt fraction. This distribution confirms the soil's classification as silty sand (SM) under SUCS, consistent with the site's sandy–clayey profile. The smooth curvature and absence of abrupt inflections suggest a well-graded granular material suitable for numerical modeling and retaining wall design.

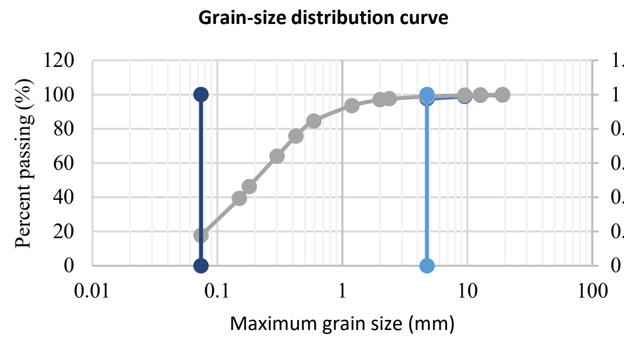

Fig.3. Particle size distribution curve

The natural moisture content of the soil was 31.62%, a relatively high value for a granular material. This condition reduces effective stress, increases the potential for pore-pressure buildup, and influences the soil's stiffness and drainage behavior—factors that are critical for retaining wall performance in seismic regions such as Sachaca. According to the SUCS classification, the material corresponds to a silty **sand (SM)**, consistent with the fines content observed in the grain-size distribution curve. Atterberg limits were not determined because the soil does not exhibit plasticity, which is typical of non-cohesive granular soils with moderate silt content.

3.2 Direct Shear Test

The direct shear test was conducted to determine the shear strength parameters of the soil under drained conditions. Three levels of normal stress 0.75, 1.50, and 2.25 kgf/cm²—were applied, resulting in shear stresses of 0.52, 0.92, and 1.39 kgf/cm², respectively. As shown in Figure 3, the stress–stress relationship exhibits a clear linear trend, confirming the soil's frictional behavior. From the regression line, a cohesion of 0.03 kg/cm² and an internal friction angle of 30.1° were obtained. The dry density of the sample was 1.53 g/cm³**,** consistent with the SUCS classification of silty sand (SM)**.** These parameters were used as input for the numerical modeling in PLAXIS 2D.

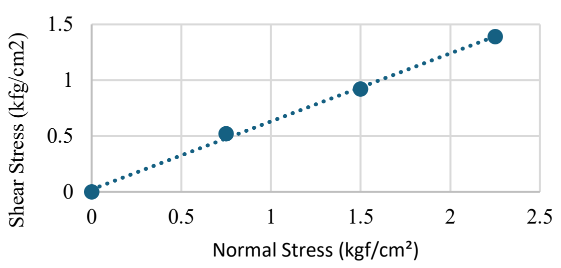

Fig. 4. Normal stress vs. shear stress graph

3.3 Modeling of the retaining wall

3.3.1 Cantilever wall (MV)

The cantilever wall was modeled in PLAXIS 2D using three geometric configurations derived from the preliminary design criteria. All models considered a total wall height of **5 m**, varying only in base width, toe length, and stem thickness to evaluate their influence on structural response. The geometric parameters used in the simulations are summarized in Table VII.

TABLE VII
PRELIMINARY DESIGN DATA FOR THE REINFORCED CONCRETE WALL

H	h	h z	B	p	a	t	b
5	1	0.6	3	0.75	0.5	1.75	0.2
5	1	0.6	3.5	0.95	0.5	2.05	0.25
5	1	0.65	4	1.10	0.55	2.35	0.3

Note: The models were developed using a wall height of 5 m.

3.3.2 The MSE wall was modeled using a uniform soil profile for the reinforced zone, retained zone, and foundation layer. This assumption reflects the site conditions in Sachaca, where the subsurface consists of a continuous deposit of silty sand (SM). The mechanical parameters used in the model are presented in Table VIII.

TABLE VIII
SOIL DATA

Parameter	Reinforced soil	Retained soil	Foundation soil
γr (kN/m³)	15	15	15
Cr (kN/m²)	2.94	2.94	2.94
φr (°)	30.1	30.1	30.1

Note: The soil maintains uniformity across all layers and throughout its entire extent.

3.3.3 Design of the MSE wall reinforced with geogrid and geodrain

The mechanically stabilized earth (MSE) wall was modeled using three geometric configurations to evaluate the influence of geogrid spacing and reinforcement length on global performance. All models were developed with a total wall height of 5 m, while the reinforcement length (L) and vertical spacing (Sv) were varied as part of the parametric study. The geometric characteristics used in the simulations are summarized in Table IX.

TABLE IX
GEOMETRY DATA

H	L	Sv	L1	Geogrid	Geodrain
5	8.3	0.4	1	BX30P	SHEET 183
5	8.2	0.6	1	BX30P	SHEET 183
5	7.6	1	1	BX30P	SHEET 183

Note: The models were developed using a wall height of 5 m.

The reinforcement system consisted of a biaxial geogrid (BX30P) placed at different vertical spacings, combined with a planar geodrain (SHEET 183) installed behind the wall to enhance pore-pressure dissipation. The mechanical and hydraulic properties of both geosynthetics, obtained from manufacturer catalogs, are presented in Table X.

TABLE X
GEODRID AND GEODRAIN PROPERTIES

Geogrid		Geodrain	
Tensile strength (kN/m)	30	Compressive strength (kN/m)	862
Thickness (mm)	1.8	Thickness (mm)	10
Aperture size (mm)	36x34	Water flow rate (L/min.m²)	6.724

Note: Data obtained from catalogs [34] and [35].

3.4 Modeling in PLAXIS 2D software

3.4.1 Cantilever Wall (MV)

The three cantilever wall configurations were modeled in PLAXIS 2D using the geometric parameters defined in Section 3.3.1. Each model incorporates the same soil profile, surcharge, and boundary conditions, varying only in base width and stem thickness to evaluate their influence on structural performance. Figures 4–6 illustrate the numerical models corresponding to MV-1, MV-2, and MV-3.

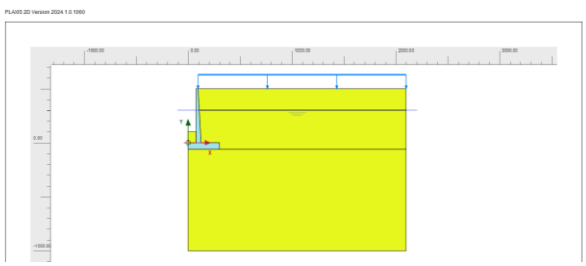

Fig. 5. Modeling of MV No. 1 in PLAXIS 2D. units on cm^{-1}

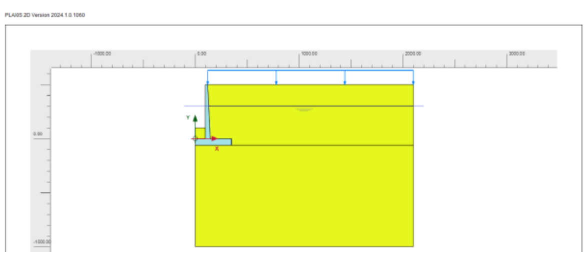

Fig. 6. Modeling of MV No. 2 in PLAXIS 2D. units on cm^{-1}

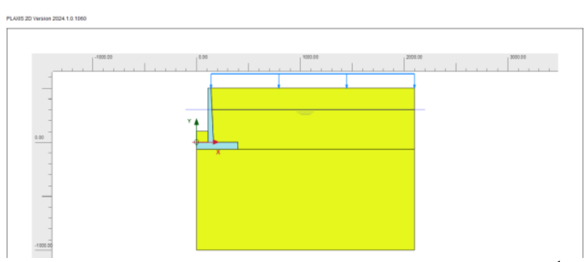

Fig. 7. Modeling of cantilever MV No. 3 in PLAXIS 2D. units on cm^{-1}

3.4.2 The MSE wall was modeled using the three reinforcement configurations described in Section 3.3.3. The variations correspond to changes in geogrid vertical spacing (Sv) and reinforcement length (L), while the geodrain remained constant in all cases. Figures 7–9 show the PLAXIS 2D models for MSE-1, MSE-2, and MSE-3, including the reinforced zone and the drainage layer.

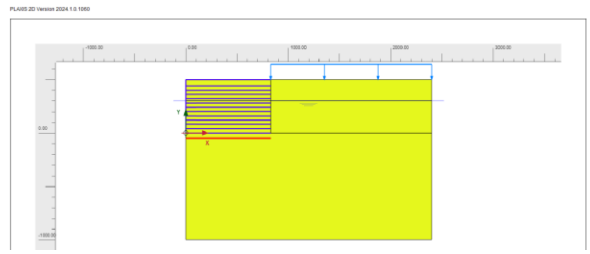

Fig. 8. Modeling of the MSE reinforced with biaxial geogrid and planar geodrain No. 1 in PLAXIS 2D. units on cm^{-1}

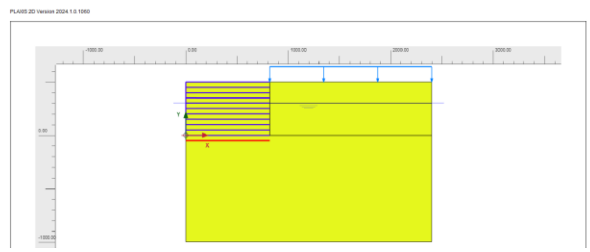

Fig. 9. Modeling of the MSE reinforced with biaxial geogrid and planar geodrain No. 2 in PLAXIS 2D. units on cm^{-1}

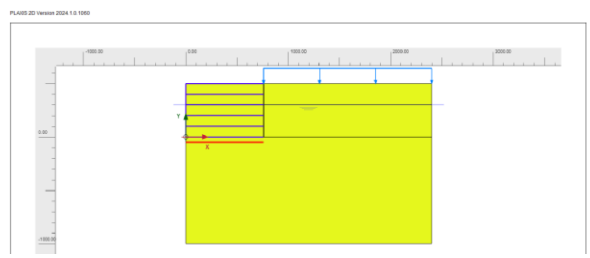

Fig. 10. Modeling of the MSE reinforced with biaxial geogrid and planar geodrain No. 3 in PLAXIS 2D. units on cm^{-1}

3.4.3 Final results of the PLAXIS 2D modeling

Tables XI and XII summarize the displacements, deformations, and pore pressures obtained from the numerical analyses for both wall types.

TABLE XI
RESULTS OF THE CANTILEVER WALLS

Wall	Cantilever		
Result	1	2	3
Displacement (cm)	0.0045	0.0026	0,0038
Deformation (cm)	$2.4x10^{-5}$	$2.5x10^{-6}$	$5x10^{-6}$
Pore pressure (kN/cm²)	$0.0223x10^{-6}$	$0.0209x10^{-6}$	$0.0212x10^{-6}$

Note: Summary of the PLAXIS 2D output

TABLE XII
RESULTADOS DE LOS MSE CON GEOMALLA Y GEODREN

Wall	MSE		
Result	1	2	3
Displacement (cm)	0,25	0,25	0,25
Deformation (cm)	$5.67x10^{-4}$	$6.35x10^{-4}$	$4{,}53x10^{-4}$
Pore pressure (kN/cm²)	$0.01678x10^{-6}$	$0.01679x10^{-6}$	$0.02401x10^{-6}$

Note: Summary of the PLAXIS 2D output

TABLE XIII
VENTAJAS Y DESVENTAJAS TÉCNICAS

	MV	MSE
Comportamiento estructural	Rigido; limitado por la resistencia del concreto	Flexible, diseñado para deformarse y disipar energia
Control de Deformaciones	Menores desplazamientos bajo cargas estáticas.	Mayor reducción de desplazamientos en suelos granulares.
Requerimientos de Espacio	Require poco espacio detrás del muro	Necesita gran área para la longitud de las malas
Análisis PLAXIS 2D	Concentra esfuerzos maximos en el talon y pie de Ia base	Logra una distribución uniforme de presiones en el suelo
Aspectos Constructivos	Proceso convencional: requiere encofrado y curado	Proceso rápido, requiere control estricto de material de refieno

IV. DISCUSSION

The cantilever walls presented substantially lower displacements and deformations than the MSE walls, a response consistent with the greater stiffness and rigidity of reinforced concrete. In contrast, the MSE walls developed lower pore pressures, a direct result of the planar geodrain incorporated into the reinforced soil mass. This behavior demonstrates the effectiveness of the drainage system in dissipating hydraulic pressures and improving the wall’s hydraulic performance.

The results obtained for the cantilever wall show an average displacement of 0.00363 cm under sandy–clayey soil conditions. This value is significantly lower than that reported by Yavan et al. [12], who obtained 0.497 cm for a 5 m-high wall, which represents a value 136.91 times greater than that observed in the present study. Similarly, Al Kahfaji et al. [18] recorded a maximum displacement of 0.13 cm in a soil with a cohesion of 0.2 kN/m², equivalent to a value 35.81 times higher than the average displacement obtained in this work.

In the case of geogrid-reinforced walls, an average displacement of 0.25 cm was obtained with a moisture content of 31.62%. This value is considerably lower than that reported by Wang et al. [10], who documented a displacement of 4 cm for a geogrid-reinforced wall under a moisture content of 16%, that is, 16 times greater than that recorded in the present analysis.

On the other hand, the MSE wall reinforced with biaxial geogrid and planar geodrain exhibited a deformation of 5.51×10^{-4} cm under a surcharge of 500 kg/m². This value is 1923.77 times lower than the deformation of 1.06 cm reported by Abdelrahman et al. [16] for a mechanically stabilized earth wall with gabions and geogrid subjected to a surcharge of 60 kN/m².

When directly comparing both typologies, the results show greater efficiency for the cantilever wall, which presents displacements and deformations of 3.63×10^{-3} cm and 1.05×10^{-5} cm, respectively. In contrast, the MSE wall with geogrid and geodrain exhibits displacements of 0.25 cm and deformations of 5.517×10^{-4} cm, confirming that the cantilever wall offers better performance against lateral movements.

Finally, regarding pore pressure, the MSE wall shows an average value of 1.919×10^{-8} kN/cm², lower than that recorded in the cantilever wall (2.147×10^{-8} kN/cm²). This indicates that pore pressure in the cantilever wall is 1.12 times higher, highlighting the greater efficiency of the MSE system in dissipating hydraulic pressures.

Several limitations were identified in the study. The numerical modeling was performed exclusively in PLAXIS 2D using the Mohr-Coulomb constitutive model and the experimental parameters reported in Tables VII-XIII. The original project file (p2dx) and the exact software version (Bentley PLAXIS Ultimate 2024.1.0) are not included in the submission package. Therefore, small variations in PLAXIS versions or numerical configurations (element type, mesh size, convergence criteria) can produce differences in the magnitude of the results. Furthermore, comparisons with previous studies were not always performed under standardized conditions (differences in cohesion, moisture content, surcharge, and reinforcement modeling), which may explain the discrepancies in displacements and deformations. The geodrainage was modeled as a layer with equivalent permeability, which is a simplification compared to a detailed representation of the flow within the actual geodrainage. To mitigate these effects, the input parameters, analysis sequence, and convergence checks were thoroughly documented; sensitivity tests (mesh refinement and variation of E and k) were also performed to verify the stability of the observed trends. The input files and meshes are available to interested reviewers or researchers upon justified request.

V. CONCLUSIONS

The modeling of the mechanical behavior of cantilever retaining walls and MSE walls reinforced with biaxial geogrid and planar geodrain using PLAXIS 2D made it possible to evaluate and compare their performance in the sandy–clayey soil of Sachaca, characterized by a moisture content of 31.62%, a density of 1.53 g/cm³, a cohesion of 0.03 kg/cm², and a friction angle of 30.1°. The results show that the cantilever wall exhibits lower deformations and displacements, making it the most efficient alternative in terms of stiffness and control of lateral movements. In contrast, the MSE wall demonstrated a greater capacity for pore-pressure dissipation, achieving a performance 1.12 times higher in this aspect.

These findings provide relevant criteria for the optimized design of retaining structures in granular soils, particularly in contexts where pore pressure is a critical factor for stability. It is recommended to further investigate the behavior of the MSE wall with geogrid and geodrain under more demanding pore-pressure conditions, incorporating advanced simulations and experimental or construction-based validations that may expand the understanding of its long-term performance. The parameters and analysis sequence are documented; the PLAXIS input files are available to reviewers upon request, facilitating verification and reproduction of the results.

REFERENCES

[1] R. L. Schuster y A. K. Turner, *LANDSLIDES: INVESTIGATION AND MITIGATION*, 1 era. Estados Unidos: Transportation Research Board National Research Council, 1996.

[2] M. V. Mata, N. Sosa, y S. Lima, *Dirección de Geología Ambiental y Riesgo Geológico Equipo de Investigación*, Primera., vol. INGEMMET. LIma, 2021.

[3] José Colque, «Muro de contención en complejo de Sachaca implica riesgo para pobladores», Arequipa, ene. 2023. Accedido: 13 de abril de 2025. [En línea]. Disponible en: https://diarioelpueblo.com.pe/2023/01/24/muro-de-contencion-en-complejo-de-sachaca-implica-riesgo-para-pobladores/

[4] j Calavera, *Muros de contención y muros de Sótano*, 2DA ed. Madrid: INTEMAC, instituto tecnologico de materiales y construcciones, 1989.

[5] M. W. Falah y H. H. Muteb, «Evaluation of mechanically stabilized earth retaining walls for different soil–structure interaction methods: A review», *DE GRUYTER Open Engineering*, vol. 14, sep. 2024, doi: 10.1515/eng-2022-0535.

[6] N. Zampirolli, A. D. Farfán, y P. C. de A. Maia, «Three-dimensional numerical analysis of the effect of foundation stiffness on soil-structure interaction», *Soils and Rocks*, vol. 47, n.º 4, pp. 1-11, oct. 2024, doi: 10.28927/SR.2024.000424.

[7] A. Johari y M. Maroufi, «System reliability analysis of geogrid reinforced retaining wall using random finite element method», *Transportation Geotechnics*, vol. 48, sep. 2024, doi: 10.1016/j.trgeo.2024.101316.

[8] S. K. Shukla, N. Sivakugan, y B. M. Das, «Fundamental concepts of soil reinforcement - An overview», *International Journal of Geotechnical Engineering*, vol. 3, n.º 3, pp. 329-342, jul. 2009, doi: 10.3328/IJGE.2009.03.03.329-342.

[9] H. Arqueñiva y R. Romero, «Estudio y evaluación comparativa entre suelos reforzados con geomalla y muros de concreto armado para la estabilización de taludes de carreteras», *Revista Científica Ciencias Ingenieriles*, vol. 1, n.º 1, pp. 20-32, jul. 2021, doi: 10.54943/ricci.v1i1.202.

[10] Z. Wang, G. Zhang, G. Yang, Y. Qin, y S. Zhou, «Experimental study on geogrid-soil interface properties based on pullout tests: A case study», *Case Studies in Construction Materials*, vol. 22, jul. 2025, doi: 10.1016/j.cscm.2025.e04376.

[11] Y. Zhu, Z. Zhan, Y. Hong, P. Guo, M. He, y R. Chen, «Experimental Study on Mechanical and Deformation Characteristics of Geogrid-Reinforced Soil Retaining Walls», *International Journal of Geosynthetics and Ground Engineering*, vol. 10, n.º 5, oct. 2024, doi: 10.1007/s40891-024-00585-9.

[12] O. YAVAN, T. TABAK, y A. TUNCAN, «BEHAVIOR OF RETAINING WALLS CONSTRUCTED IN THE SATURATED CLAY AND WATER-SATURATED SAND SOILS UNDER THE DYNAMIC LOADS», *Kırklareli Üniversitesi Mühendislik ve Fen Bilimleri Dergisi*, vol. 8, n.º 2, pp. 253-272, dic. 2022, doi: 10.34186/klujes.1183631.

[13] K. Naga *et al.*, «Parametric Analysis and Design of Cantilever Retaining Walls Under Different Soil Conditions», *Internacional journal of engineering research and tecnology*, mar. 2024, doi: 10.17577/IJERTV13IS030078.

[14] M. S. Hammad, M. A. Hassan, y A. L. Fayed, «Study of the global factor of safety for mechanically stabilized earth wall (MSE) using numerical modelling», en *Materials Research Proceedings*, Association of American Publishers, 2025, pp. 475-485. doi: 10.21741/9781644903414-52.

[15] A. Tomar, J. Lohar, y N. Shrivastava, «Parametric Study of Mechanically Stabilised Earth Wall using PLAXIS», en *IOP Conference Series: Earth and Environmental Science*, Institute of Physics, 2024. doi: 10.1088/1755-1315/1326/1/012126.

[16] G. E. Abdelrahman, Y. G. Youssef, y A. Emad Abdeltawab, «3D numerical analysis of corner mechanically stabilized earth walls», *HBRC Journal*, vol. 20, n.º 1, pp. 179-204, 2024, doi: 10.1080/16874048.2024.2309821.

[17] U. C. Sari, M. N. Sholeh, y I. Hermanto, «The stability analysis study of conventional retaining walls variation design in vertical slope», en *Journal of Physics: Conference Series*, Institute of Physics Publishing, feb. 2020. doi: 10.1088/1742-6596/1444/1/012053.

[18] R. S. Al-Khafaji, M. A. Al-Obaydi, y Q. N. Al-Saffar, «Effect of surcharge load location on the behavior of cantilever retaining wall», *J Mech Behav Mater*, vol. 32, n.º 1, ene. 2023, doi: 10.1515/jmbm-2022-0247.

[19] L. Wang *et al.*, «Comparative study on seismic performances of vertical waste tire-faced retaining walls (unreinforced/reinforced)», *Yantu Gongcheng Xuebao/Chinese Journal of Geotechnical Engineering*, vol. 45, n.º 2, pp. 273-282, feb. 2023, doi: 10.11779/CJGE20211400.

[20] C. F. Schmidt, P. P. M. S. Dos Anjos, I. Steinmeyer, M. C. R. Cleto, y E. M. Andrade, «Mechanically stabilized wall (MSW) with geogrids as complement of partially executed anchored wall», *Soils and Rocks*, vol. 46, n.º 4, oct. 2023, doi: 10.28927/SR.2023.004623.

[21] C. V. S. Benjamim, B. S. Bueno, y J. G. Zornberg, «Field monitoring evaluation of geotextile-reinforced soil-retaining walls», *Geosynth Int*, vol. 14, n.º 2, pp. 100-118, 2007, doi: 10.1680/gein.2007.14.2.100.

[22] C. Doulala-Rigby y A. Pérez, «40 años de estructuras de suelo reforzadas con geomalla de polietileno de alta densidad (HDPE): Los muros más altos de Latinoamérica a los Emiratos Árabes Unidos», *South Florida Journal of Development*, vol. 2, n.º 2, pp. 2729-2739, jun. 2021, doi: 10.46932/sfjdv2n2-126.

[23] B. Cai, X. Cai, S. Li, X. Huang, Y. Zhang, y C. Xiao, «Experimental study of shaking table for reinforced soil retaining walls: Analysis of tiered configuration effects», *Soil Dynamics and Earthquake Engineering*, vol. 188, ene. 2025, doi: 10.1016/j.soildyn.2024.109076.

[24] M. Cholewa y K. Plesiński, «Performance comparison of geodrain drainage and gravel drainage layers embedded in a horizontal plane», *Materials*, vol. 14, n.º 21, pp. 1-11, nov. 2021, doi: 10.3390/ma14216321.

[25] K. M. Morsy y H. Thakeb, «Comparative evaluation of the environmental impacts of geosynthetic Mechanically Stabilized Earth walls», *J Clean Prod*, vol. 374, p. 133912, nov. 2022, doi: 10.1016/J.JCLEPRO.2022.133912.

[26] R. Lajer, T. Klitgaard Person, M. Strømgaard Hansen, y T. Dambo Nielsen, «Deep foundation for high rise in tricky soil conditions and surroundings in Scandinavia – Walkthrough of various high-rise projects from initial geology to final execution and everything in between», *Geomechanics and Tunnelling*, vol. 18, n.º 2, pp. 112-123, abr. 2025, doi: 10.1002/geot.202400073.

[27] S. P. Kakuturu, M. Xiao, y M. Kinzel, «Effects of Maximum Particle Size on the Results of Hydrometer Tests on Soils», *Geotechnical Testing Journal*, vol. 42, n.º 4, pp. 945-965, jul. 2019, doi: 10.1520/GTJ20170236.

[28] N. Almutawa y W. Eid, «Soil moisture content estimation using active infrared thermography technique: An exploratory laboratory study», *Kuwait Journal of Science*, vol. 50, n.º 3, pp. 399-404, jul. 2023, doi: 10.1016/j.kjs.2022.11.001.

[29] X. Zhao, W. D. Zhu, Y. H. Li, M. Li, y X. Y. Li, «Review, classification, and extension of classical soil-structure interaction models based on different superstructures and soils», *Thin-Walled Structures*, vol. 173, p. 108936, abr. 2022, doi: 10.1016/J.TWS.2022.108936.

[30] A. Soltani y B. C. O'kelly, «Reappraisal of the astm/aashto standard rolling device method for plastic limit determination of fine-grained soils», *Geosciences (Switzerland)*, vol. 11, n.º 6, jun. 2021, doi: 10.3390/geosciences11060247.

[31] S. L. Huanca, J. C. L. Huanca, y R. A. L. Vilca, «A Rational Interpretation of Laboratory Direct Shear Test Results for Soils», *Springer Nature Link*, pp. 340-350, may 2023, doi: 10.1007/978-3-031-31007-2_31.

[32] B. M. Das, *Fundamentos de ingeniería geotécnica Cuarta edición*, Cuarta. Cicinnati: Cengage Learning, 2015.

[33] GEOSISTEMAS PAVCO, *MANUAL DE DISEÑO CON GEOSINTÉTICOS*, Octava edición. Bogota Colombia: Zetta Comunicadores S.A., 2009.

[34] Arpimix, «Presentaciones disponibles de la geomalla biaxial de polipropileno», Geosinteticos Arpimix. Accedido: 21 de abril de 2025. [En línea]. Disponible en: https://arpimix.com/productos/geomalla-biaxial-de-propileno/

[35] Sitedrain, «DRENAJES DE CAPA PREFABRICADOS», Amererican Wick Drain, abr. 2025.